

Redox ratio of mitochondria as an indicator for the response of photodynamic therapy

Zhihong Zhang

Huazhong University of Science and Technology
Key Laboratory of Biomedical Photonics
Ministry of Education
Wuhan, Hubei 430074, P.R. China
and
University of Pennsylvania Medical School
Department of Biochemistry and Biophysics
Philadelphia, Pennsylvania 19104

Dana Blessington

University of Pennsylvania Medical School
Department of Biochemistry and Biophysics
Philadelphia, Pennsylvania 19104

Hui Li

University of Pennsylvania Medical School
Department of Radiology
Philadelphia, Pennsylvania 19104

Theresa M. Busch

University of Pennsylvania Medical School
Department of Radiation Oncology
Philadelphia, Pennsylvania 19104

Jerry Glickson

University of Pennsylvania Medical School
Department of Radiology
Philadelphia, Pennsylvania 19104

Qingming Luo

Huazhong University of Science and Technology
Key Laboratory of Biomedical Photonics
Ministry of Education
Wuhan, Hubei 430074, P.R. China

Britton Chance

University of Pennsylvania Medical School
Department of Biochemistry and Biophysics
Philadelphia, Pennsylvania 19104

Gang Zheng

University of Pennsylvania Medical School
Department of Radiology
Philadelphia, Pennsylvania 19104
E-mail: Gang.Zheng@uphs.upenn.edu

Abstract. The effect of photodynamic therapy (PDT) treatment on the metabolic state of tumor mitochondria is investigated by imaging of tumor redox status. PDT is performed using the photosensitizer pyropheophorbide-2-deoxyglucosamide (Pyro-2DG), which utilizes the glucose import pathway. It is found that Pyro-2DG-induced PDT resulting in a highly oxidized state of tumor mitochondria. This is determined from the redox ratio changes derived from the intrinsic oxidized flavoprotein (Fp) and reduced pyridine nucleotide (PN) [i.e., reduced nicotinamide adenine dinucleotide (NADH)] fluorescence signals observed using a cryoimager. Thus, the redox ratio is a sensitive indicator for providing reliable and informative measurements of PDT-induced tissue damage. In the PDT treated region of the tumor, highly oxidized flavoprotein and diminishing NADH fluorescence is detected, suggesting that flavoprotein and NADH are oxidized by singlet oxygen produced in the photosensitization process. © 2004 Society of Photo-Optical Instrumentation Engineers. [DOI: 10.1117/1.1760759]

Keywords: redox ratio; photodynamic therapy; pyropheophorbide-2-deoxyglucosamide; 9L glioma; cryoimager.

Paper 03105 received Aug. 11, 2003; revised manuscript received Dec. 2, 2003; accepted for publication Dec. 19, 2003.

1 Introduction

Photodynamic therapy (PDT) involves the photoexcitation of a tissue-localized sensitizer and subsequent energy transfer from the excited triplet state photosensitizer to molecular oxygen, resulting in the generation of singlet oxygen.¹ Subsequent oxidation-reduction reactions can also produce superoxide anions, hydrogen peroxide and hydroxyl radicals.¹ Singlet oxygen is extremely reactive and exhibits a lifetime of 0.03 to 0.18 μ s in tissues.² This restricts its activity to a spherical volume, 10 nm in diameter, centered at its point of production.³ Because singlet oxygen reacts so rapidly, PDT-induced oxidative damage is highly localized to regions no

larger in diameter than the thickness of a cell membrane. Due to the hydrophobic character of most photosensitizers,³ photodynamic damage is most likely confined to targets near to or within hydrophobic regions of the cell. Mitochondria, lysosomes, plasma membrane, and nuclei of tumor cells have been evaluated as potential PDT targets, along with the tumor vasculature.¹ Vascular shutdown is clearly an important aspect⁴ of PDT, but since both vasculature and tumor are composed of individual cells, the identification of an optimal sub-cellular target remains relevant.¹

Numerous reports have implicated mitochondria as important targets⁵ of PDT. Photosensitizers that localize to mito-

Address all correspondence to Dr. Gang Zheng, Univ. of Pennsylvania, Dept. of Radiology, Philadelphia, PA 19104. E-mail: Gang.Zheng@uphs.upenn.edu

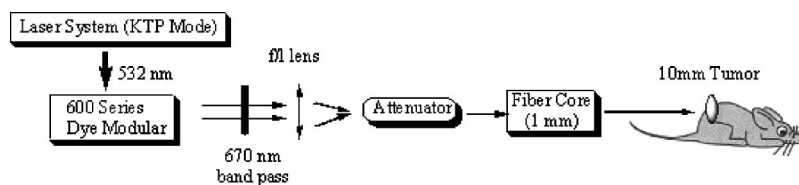


Fig. 1 PDT laser setup for evaluating Pyro-2DG in 9L glioma bearing rat.

chondria are reported to be more efficient in killing cells than those that localize at the other cellular sites.^{6,7} In response to PDT with various mitochondrion-bound photosensitizers, cytochrome *c* is released from the intermembrane space into the cytosol, where it most likely forms a complex with cytoplasmic apoptosis activation factor-1 (APAF-1) to initiate the caspase cascade in the final stages of apoptosis.^{8,9} Often the first event observed in PDT-induced apoptosis is a dissipation of the mitochondrial transmembrane potential ($\Delta\Psi_m$). PDT with the mitochondrion-localized photosensitizers hypericin or hypocrellin, induces¹⁰ a rapid decrease in $\Delta\Psi_m$.

The mitochondria provide a “consumer report” on the intracellular oxygen tension and the level of metabolic activity, producing a large number of spectroscopic signals of the normoxic-anoxic transition. Prominent among them are the increase of fluorescence of reduced (NADH) over oxidized (NAD⁺) pyridine nucleotide and of oxidized over reduced flavoprotein. Thus, the use of two fluorophores, the oxidized flavoprotein (Fp) and the reduced pyridine nucleotide (PN), is especially attractive for two reasons. First, the measurement of the ratio of fluorescence, rather than of absolute values, makes much less stringent demands on the instrumentation and is complicated far less by interference from other pigments. Second, and most important for biochemical studies, the measurement of the ratio of the signals for oxidized Fp and reduced PN provides an index for measurement of the redox status of the mitochondrial matrix space and of steady state mitochondrial metabolism.

We recently¹¹ synthesized a new photosensitizer, proporphorbide-2-deoxyglucosamide (Pyro-2DG). Confocal fluorescence imaging studies showed that Pyro-2DG is a mitochondria-localized photosensitizer.¹² In addition, its distribution in tumor tissue is highly correlated with the redox ratio of tumor mitochondria.¹² In this study, we used the cryoimaging technique to monitor the PDT effect of Pyro-2DG on the redox ratio of the tumor.

2 Materials and Methods

2.1 9L-Glioma-Bearing Rat Model Preparation

9L glioma cells, which were obtained from Dr. Sydney Evans' laboratory in the Department of Radiation Oncology of the University of Pennsylvania, were cultured in modified Eagle's medium (MEM) supplemented with 15% newborn calf serum (NCS), 100 U/ml penicillin-streptomycin. Cells were grown at 37 °C in an atmosphere of 5% CO₂ in a humidified incubator. For the 9L glioma bearing rat model, 2 × 10⁶/0.2 ml 9L glioma cells were implanted in the flanks of male Fisher 344 rats (150 to 200 g) via subcutaneous injection. In 10 days the tumor grew to 1 cm in diameter.

2.2 Photosensitizer and PDT Treatment

Pyro-2DG was synthesized following a previously described procedure.¹¹ The 9L glioma bearing rat was fasted for 24 h and then anesthetized via an intraperitoneal injection of ketamine (75 mg/kg) and xylazine (10 mg/kg). Pyro-2DG (2 mL, concentration: 0.25 mg/mL) was administered via tail vein infusion over a period of 1 h (dose: 2.5 mg/kg). The rat was subjected to PDT 30 min after completion of the Pyro-2DG infusion. All PDT processes were carried out in 38 min to a total dose of 175 J/cm² delivered at a fluence rate of 75 mW/cm². The light was delivered at 670 nm (based on the absorption and emission spectra of Pyro-2DG; see Fig. 2 in Sec. 2.3) using a laser system consisting of a KTP-YAG-pumped dye module (Laserscope, San Jose, California). The power output was measured with a coherent laser mate photodiode detector (Model # LM-2 VIS, Serial #TZ52) with a Field Master power meter (model: Field Master, serial # 10T46). For proof of principle, we designed a “point treatment” protocol for evaluating PDT response of Pyro-2DG (see Fig. 1). Instead of irradiating the whole tumor area (1 cm in diameter), we applied a cut end fiber with a 1-mm core that is not implanted in the tumor. To minimize movement of the light beam, the animal was anesthetized during PDT, and the optical fiber core was clamped to a disk glued directly to the skin on top of the tumor. This point treatment procedure is designed for two purposes: (1) to enable the adjacent untreated tumor region along with the normal tissue region to serve as internal controls and (2) to evaluate possible bystander effects. Immediately after PDT treatment, the anesthetized rat was immersed in precooled isopentane (−150 °C) for 3 min and then transferred to liquid nitrogen (−196 °C).

2.3 Fluorescent Imaging of Tumors with 3-D Cryoimager^{13,14}

Tumor tissues were surgically excised, embedded in an ethanol-glycerol-water mixture (freezing point: −30 °C), and mounted in the cryoimager for 3-D surface fluorometric scanning. The frozen tumor sample was ground flat and then further ground to obtain images every 300 μm from the top surface to the bottom of the tumor. A bifurcated optical fiber bundle (seven quartz fibers, 70 μm core diameter for each, 0.34 numerical aperture, one fiber for emission in center, six fibers for excitation around the emission fiber) stepped across the tissue at a fixed distance of 100 μm from the surface. The excitation and emission filters were designed in accordance with the absorption and emission spectra of each substance and the emission spectrum of the mercury arc lamp (see Fig. 2). Using a mercury arc lamp as the excitation light source, the fluorescent signals of Fp (filters: Ex: 440DF20, Em: 520DF40), PN (filters: Ex: 365HT25, Em: 455DF70), and

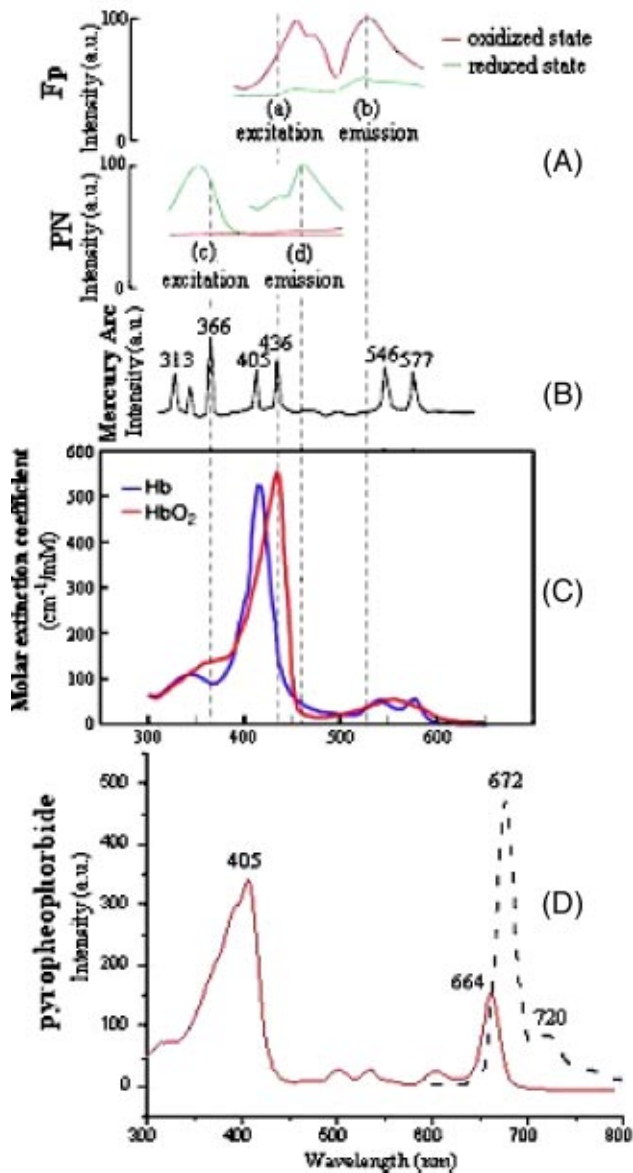


Fig. 2 (A) Excitation and emission spectra of Fp and PN in the oxidized and reduced state, (B) emission spectra of the mercury arc lamp, (C) absorption spectra of oxy- and deoxyhemoglobin, and (D) excitation and emission spectra of Pyro-2DG. Figures 2(A)–2(C) reproduced with permission from Ref. 14.

Pyro-2DG (filters: Ex: 405DF40, Em: 700ALP) were imaged for each depth of the tumors. The scanning was performed at 128×128 steps that covered a 1.024×1.024 -cm² area ($80 \mu\text{m}$ in-plane resolution). The fluorescence signals were automatically digitized and recorded on a PC. The redox ratio of PN/(Fp+PN) and Fp/(Fp+PN) calculated with MATLAB represented the reduced state and oxidized state of the mitochondria, respectively.

3 Results

The intrinsic and extrinsic fluorescent signals of 9L glioma after PDT treatment (number of rats, $n=3$) were scanned with the cryoimager. The fluorescence images of Fp, PN, and Pyro-2DG, the redox ratio images of PN/(Fp+PN) and Fp/(Fp

+PN), as well as their corresponding histograms are shown in Figs. 3(a) to 3(e), respectively. The size of each fluorescent image and redox ratio image is 1.024×1.024 cm² (each pixel being $80 \times 80 \mu\text{m}$); the color indicates the intensity of the detected light at a particular wavelength. The x and y axes of the histograms represent, respectively, the relative fluorescent intensity or redox ratio and the corresponding frequency of occurrence of that fluorescent intensity or redox ratio. All histograms correspond to their respective tumor regions. For comparison, a photographic image of the frozen tissue block is shown in Fig. 3(f).

As shown in these images, one of the distinctive regions in this tumor sample is the skin [region 3 marked in Fig. 3(d)], which clearly defines the tumor margin. As for the tumor tissue, there are two distinctive regions. The first area (region 1) is shown in the right, upper half of the images that appears to be unaffected by light treatment. The second area (region 2) is located in the left, lower half of the images that surrounds the region irradiated with light [marked as the black circle in Fig. 3(a)]. The distinction between two tumor regions seems to be consistent with the bimodal distribution of their histograms, indicating that one peak of the histograms was attributed to the PDT response region and the other originated from the unaffected tumor region. As shown in Fig. 3(e), region 2 has a higher Fp/(Fp+PN) ratio (peak value of 0.8, mean value of 0.82 ± 0.06), whereas region 1 has a significantly lower Fp/(Fp+PN) ratio (peak value of 0.5), indicating that region 2 is highly oxidized. Since the Fp/(Fp+PN) ratio image is derived from the fluorescence images of Fp and PN detected individually, the high Fp/(Fp+PN) ratio clearly is the result of the strong Fp fluorescent signal and the weak PN signal of region 2, as shown in Figs. 3(a) and 3(b). As a result of PDT treatment, most of the flavoproteins were converted to their oxidized state, yielding strong Fp fluorescence signal. The diminished PN signal was presumably due to the oxidation of NADH and possibly the quenching by hemoglobin.¹⁵ As expected, these data are also consistent with the observation of a reverse bimodal PN/(Fp+PN) ratio distribution in these regions. In addition, the bimodal distribution of the redox ratio corresponds well to the bimodal distribution of Pyro-2DG fluorescence intensity. The highly oxidized region 2 shows both a high Fp/(Fp+PN) ratio and a weak Pyro-2DG fluorescence signal, suggesting that the light treatment induced Pyro-2DG photobleaching in this region. Another important observation is the appearance of hemorrhage in the light-photographed tumor [Fig. 3(f)]. We attribute this hemorrhage to PDT-induced vascular damage. These images also demonstrate that the Fp fluorescence signal was strong enough to overcome hemoglobin-induced fluorescence quenching in the hemorrhage-containing region. Interestingly, the high Fp/(Fp+PN) ratio displayed in region 2 is not restricted to the irradiated region (0.1 cm in diameter) but also extends to the surrounding area about 0.5 cm from the center of the irradiated zone. This observation may be explained by the light diffusion in tumor tissue.

To confirm the correlation between the high Fp/(Fp+PN) ratio and PDT response, we performed three sets of control experiments, including drug control (Fig. 4, top row, tumor + Pyro-2DG, no irradiation), tumor control (Fig. 4, bottom row, tumor alone), and PDT control (Fig. 5, tumor+irradiation, no Pyro-2DG). To confirm that the strong oxidized Fp signal in

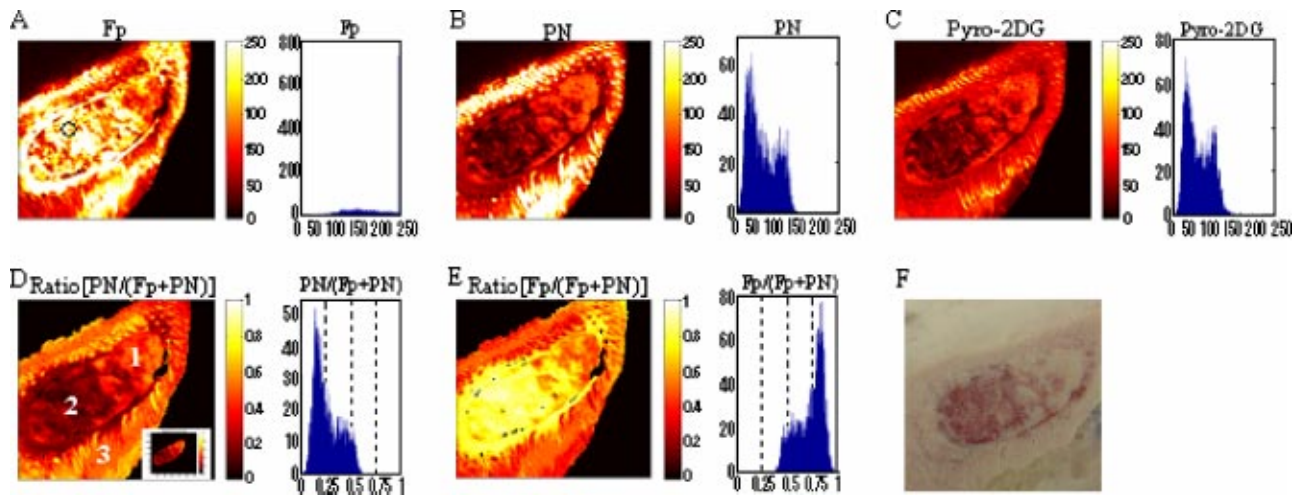


Fig. 3 Images of 9L glioma after Pyro-2DG PDT treatment obtained at a depth of 900 μm below the surface: (a), (b), and (c) the fluorescent images of Fp, PN, and Pyro-2DG of the tumor, respectively; (d) and (e) $\text{PN}/(\text{Fp}+\text{PN})$ and $\text{Fp}/(\text{Fp}+\text{PN})$ ratio images of the tumor, respectively, where the histograms of tumor are shown at the right side of each image and come from the tumor region [see the small image at the right corner of (d)]; and (f) photographic image taken by the digital camera. The size of each fluorescent image and redox ratio image is 1.024×1.024 cm. The x and y axes of the images represent the number of the pixels scanned (128×128 pixels for each image) and the color indicates the fluorescent intensity or redox ratio of the tissues. The x and y axes of the histograms represent, respectively, the relative fluorescent intensity or redox ratio and the corresponding frequency of occurrence of that fluorescent intensity or redox ratio. All histograms correspond to their respective tumor regions.

the hemorrhagic area is the result of PDT treatment, Pyro-2DG was administrated to a 9L glioma rat with an uncharacteristic large hemorrhage located in the center of the tumor as the drug control (Fig. 4, top row). Unlike the PDT-induced hemorrhage found in Fig. 3, the $\text{Fp}/(\text{Fp}+\text{PN})$ ratio in these large hemorrhagic regions was processed as the background signal since the fluorescent signals of Fp and PN were barely detectable and were either lower than or similar to the background. This is presumably due to the hemoglobin quenching effect for both Fp and PN fluorescence signal. Using this procedure, the existing hemorrhagic regions in the untreated animals can be distinguished from the PDT-induced hemorrhagic region in the PDT treated animals. Note that the $\text{Fp}/(\text{Fp}+\text{PN})$ ratio (peak value at 0.5, mean value of 0.50 ± 0.09) from the normal growth tumor region of the untreated animal (see Fig.

4, top row, columns 1 and 2) was similar to what was observed in the non-PDT responding area in the PDT treated animal (region 1 marked in Fig. 3). This further demonstrates that the dramatic increase of the $\text{Fp}/(\text{Fp}+\text{PN})$ ratio is induced by PDT treatment.

The relationship between a high $\text{Fp}/(\text{Fp}+\text{PN})$ ratio and PDT-induced oxidative damage was further examined using a tumor control (no Pyro-2DG, no irradiation) that contained small necrotic regions. The mean value of $\text{Fp}/(\text{Fp}+\text{PN})$ ratio of this tumor was determined as 0.53 ± 0.06 . As shown in the bottom row of Fig. 4, the redox ratio of a necrotic region is very similar to the characteristic redox ratio of the PDT response region (region 2 marked in Fig. 3), confirming the oxidative damage caused by PDT treatment. However, the necrotic region in this control rat showed no sign of hemor-

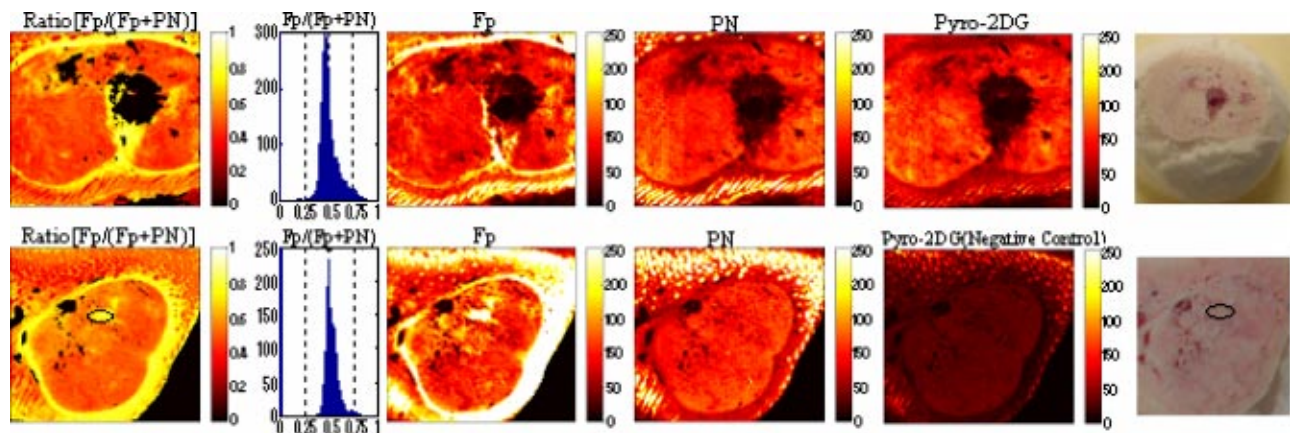


Fig. 4 Two sets of control experiments to confirm the Pyro-2DG-induced PDT response, including drug control (top row, tumor+Pyro-2DG, no irradiation) and tumor control (bottom row, tumor alone). The columns from left to right show the redox ratio images and their corresponding histograms, Fp, PN and Pyro-2DG fluorescent images, and photographic images, respectively. The oval region in the middle row is the necrosis area. The axis labels for all the fluorescence images and histograms are the same as those stated in the Fig. 3 legend.

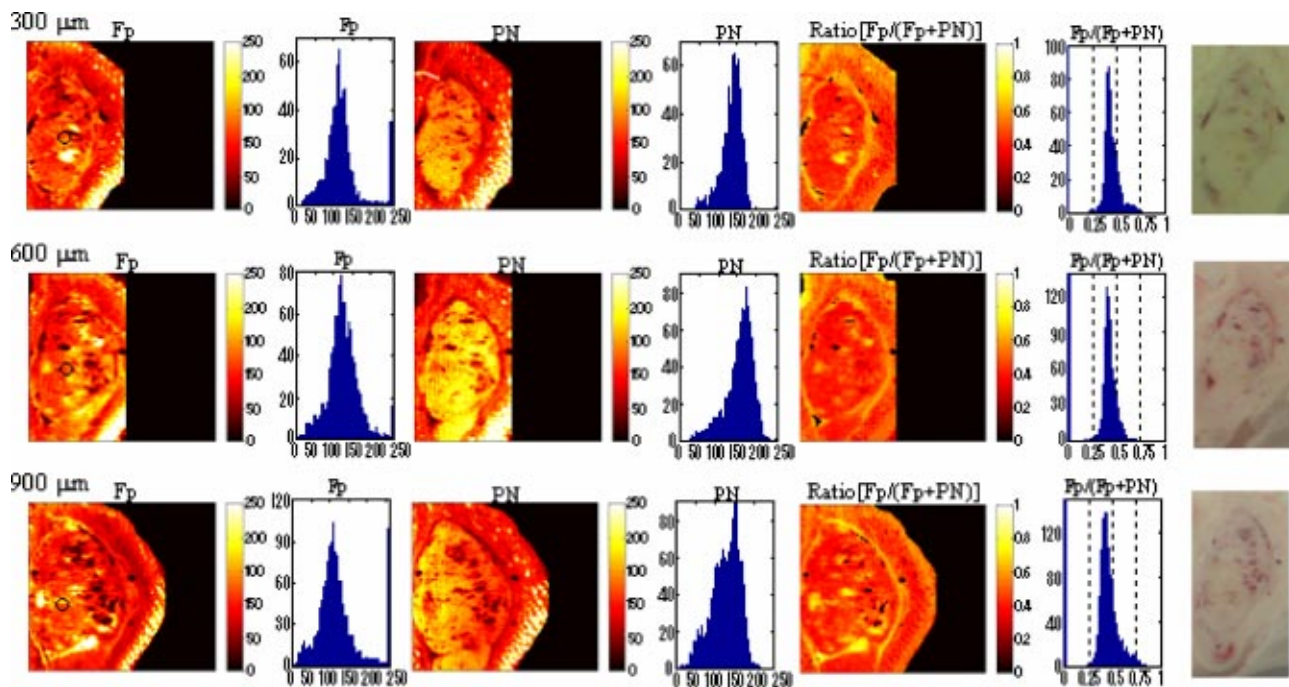


Fig. 5 Images of PDT control 9L glioma with irradiation and without Pyro-2DG. The images show the different depths at 300, 600, and 900 μm along an axis perpendicular to the tumor surface. The columns from left to right show the Fp, PN fluorescent images, redox ratio images, and their corresponding histograms and photographic images, respectively. The black circles in the first column of images are the position of irradiation region with the optic fiber. The axis labels for all the fluorescence images and histograms are the same as those stated in the Fig. 3 legend.

rhage, which further illustrated the heterogeneity of the tumor.

Finally, a PDT control experiment (tumor+irradiation, no Pyro-2DG) was performed to confirm that tumor damage was induced by the photodynamic effect of the Pyro-2DG and not by the irradiation alone. The Fp/(Fp+PN) ratio of the tumor regions was largely unchanged (peak value at 0.4, mean value of 0.45 ± 0.06) (Fig. 5). A little shift of peak value of redox ratio is due to the different metabolic state or oxygen content of tumors. This indicates that light treatment alone did not induce significant change in the redox state. Comparing the PDT-induced high oxidative state of tumors, the characteristic of *a priori* necrosis in the tumor is as follows: (1) the necrosis regions are small and disperse and (2) the hemorrhage regions display both low Fp and PN signal due to the fluorescent quenching by hemoglobin, thus, a high oxidative state was not observed. These experiments, therefore, clearly demonstrate that the change of the redox ratio in the tumor region 2 of Fig. 3 is due to Pyro-2DG photosensitization.

The data described in Fig. 3 were obtained 900 μm below the skin. To evaluate the PDT response of tumor and surrounding muscle tissues at various depths, the 9L glioma tumor sample was scanned from 300 to 4500 μm (bottom edge of the tumor) below the skin. The fluorescence images of Pyro-2DG at each depth and their corresponding redox ratio images and photographic images at the same depth were then displayed using MATLAB software, and some of the representative images are shown in Fig. 6. Thus, the highly oxidized state was observed consistently at each depth throughout the tumor region 2 in response to PDT treatment. The mean value of Fp/(Fp+PN) ratio determined for the whole tumor and for the PDT response regions were 0.69 ± 0.14 and 0.80 ± 0.08 , respectively.

4 Discussion

Because of the limited diffusion of $^1\text{O}_2$ from the site of its formation,¹⁶ sites of initial cell and tissue damage resulting from PDT are closely related to the location of the sensitizer.¹⁷ Many researchers have thus chosen to examine subcellular sites of PDT-induced alterations rather than to search for sites of sensitizer binding.¹ In this study, highly oxidized Fp signal from mitochondria was detected in the PDT treated 9L glioma, suggesting that the subcellular location of Pyro-2DG like that of pyropheophorbide¹⁸ was in the mitochondria. Our confocal fluorescence imaging studies with rhodamine 123 co-stain (data not shown) also indicate that Pyro-2DG is a mitochondria-localized photosensitizer.

One of the first stages of damage in both apoptotic and necrotic mechanisms is the loss of mitochondrial membrane integrity, and thereby, a loss of mitochondrial function.¹⁹ Measurement of this functional status is possible as many of the important molecules in the respiratory chain are strong optical chromophores. This was first explored in early 1960s by Chance et al.²⁰ to determine the respiratory status using the fluorescent signals of PN and Fp. PDT with mitochondrion-localized photosensitizers is also well known to inhibit respiration and oxidative phosphorylation.^{21,22} For example, photoactivated photofrin inhibited electron transport components, including succinate dehydrogenase and cytochrome *c* oxidase, and also disrupted the mitochondrial electrochemical gradient.^{23,24} 5-ALA-based PDT induced decreases in levels of cellular ATP and GTP, of the NADH/NAD⁺ ratio and of oxygen consumption.²⁵ In a recent study, Pogue et al.²⁶ showed that PDT-induced cellular death is well correlated with the NADH fluorescence both *in vitro* and *in vivo*. How-

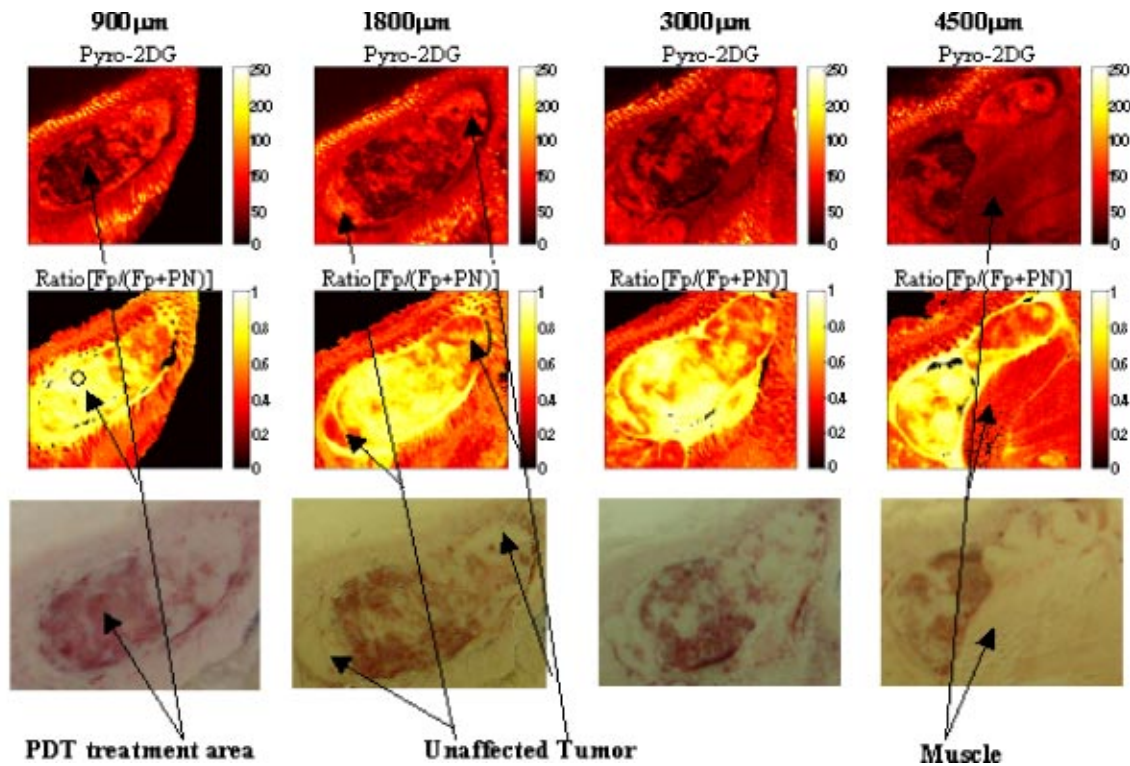


Fig. 6 Images of 9L glioma with Pyro-2DG-based PDT treatment at a series of depths. Top row: the fluorescent images of Pyro-2DG; middle row: the redox ratio of Fp/(Fp+PN); bottom row: the photographic images taken by the digital camera. The axis labels for all the fluorescence images are the same as those stated in the Fig. 3 legend.

ever, in certain cases, the decreasing reduced PN signal was probably due to fluorescent quenching by PDT induced bleeding.¹⁵

In this study, the result indicated that the redox ratio is a sensitive indicator of PDT-induced damage. The response of PN fluorescent signal to stimulation is mainly due²⁷ to mitochondrial NADH, and Fp locates only in the mitochondria. Thus, the Fp/(Fp+PN) responds to ADP and phosphate, to the citric acid cycle, to the delivery of oxygen to the mitochondria, and to their degree of activation by ADP and phosphate. The fluorescence of Fp and PN themselves may be affected by bleeding. However, detailed studies of blood added to mitochondrial suspensions showed that the ratio Fp/PN is little affected by bleeding.¹⁵ Thus, the redox ratio Fp/(Fp+PN) could effectively eliminate the measurement error induced by bleeding. Furthermore, the redox ratio calculated from oxidized Fp and reduced PN is more reliable than the measurement of absolute values of oxidized Fp and reduced PN because it makes much less stringent demands on the instrumentation and has less serious interference from hemoglobin and other pigments.¹⁸ Thus, the redox ratio is a useful indicator for providing reliable and informative measurements of PDT-induced tissue damage. In our future study, the redox ratio and Pyro-2DG fluorescent signal of tumors during PDT treatment will be measured in real time *in vivo* simultaneously. It will be useful to elucidate the relationship between PDT response and metabolic state of the tumors.

5 Conclusion

The Pyro-2DG-induced PDT resulted in a highly oxidized state of tumor mitochondria as indicated by the high Fp/(Fp

+PN) redox ratio observed by the cryoimager. Thus, the redox ratio derived from intrinsic oxidized Fp and reduced PN is applicable as a sensitive indicator for evaluating PDT-induced damage by mitochondrion-localized photosensitizers. The highly oxidized flavoprotein fluorescence and the loss of NADH fluorescence in the PDT response region is the result of direct oxidation of the NADH and flavoprotein by singlet oxygen produced in the photosensitization process.

Acknowledgments

This work was supported by National Institutes of Health (NIH) grants N01CO37119 (G.Z.), R21CA95330 (G.Z.), R01CA072895 (B.C.) and an Oncologic Foundation of Buffalo award (G.Z.). Partial supports from NIH grants R24CA83105 (J.D.G.), P20-CA86255 (J.D.G.), RR02305 (B.C.) and a grant (No. 60025514) from National Science Foundation for Distinguished Young Scholars of China (Q.L.) is also acknowledged. We are grateful to Mr. Jeremy Miles of the Department of Radiation Oncology and Mr. David Nelson of the Department of Radiology for technical assistance.

References

1. T. J. Dougherty, C. J. Gomer, B. W. Henderson, G. Jori, D. Kessel, M. Korbek, J. Moan, and Q. Peng, "Photodynamic therapy," *J. Natl. Cancer Inst.* **90**(12), 889–905 (1998).
2. M. Niedre, M. S. Patterson, and B. C. Wilson, "Direct near-infrared luminescence detection of singlet oxygen generated by photodynamic therapy in cells *in vitro* and tissues *in vivo*," *Photochem. Photobiol.* **75**(4), 382–391 (2002).
3. I. J. MacDonald and T. J. Dougherty, "Basic principles of photodynamic therapy," *J. Porphy. Phthalocyan.* **5**(2), 105–129 (2001).
4. B. W. Henderson and T. J. Dougherty, "How does photodynamic

- therapy work," *Photochem. Photobiol.* **55**(1), 145–157 (1992).
5. N. L. Oleinick, R. L. Morris, and T. Belichenko, "The role of apoptosis in response to photodynamic therapy: what, where, why, and how," *Photochem. Photobiol.* **1**(1), 1–21 (2002).
 6. D. Kessel and Y. Luo, "Mitochondrial photodamage and PDT-induced apoptosis," *J. Photochem. Photobiol., B* **42**(2), 89–95 (1998).
 7. D. Kessel, Y. Luo, Y. Deng, and C. K. Chang, "The role of subcellular localization in initiation of apoptosis by photodynamic therapy," *Photochem. Photobiol.* **65**(3), 422–426 (1997).
 8. D. J. Granville, C. M. Carthy, H. J. Jiang, G. C. Shore, B. M. McManus, and D. W. C. Hunt, "Rapid cytochrome c release, activation of caspases 3, 6, 7 and 8 followed by Bap31 cleavage in HeLa cells treated with photodynamic therapy," *FEBS Lett.* **437**(1–2), 5–10 (1998).
 9. D. Kessel and Y. Luo, "Photodynamic therapy: a mitochondrial inducer of apoptosis," *Cell Death Diff.* **6**(1), 28–35 (1999).
 10. R. Chaloupka, T. Obsil, J. Plasek, and F. Sureau, "The effect of hypericin and hypocrellin-A on lipid membranes and membrane potential of 3T3 fibroblasts," *Biochim. Biophys. Acta Biomembr.* **1418**(1), 39–47 (1999).
 11. M. Zhang, Z. H. Zhang, D. Blessington, H. Li, T. M. Busch, V. Madrak, J. Miles, B. Chance, J. D. Glickson, and G. Zheng, "Pyropheophorbide 2-deoxyglucosamide: a new photosensitizer targeting glucose transporters," *Bioconjugate Chem.* **14**, 709–714 (2003).
 12. Z. H. Zhang, H. Li, L. Qian, L. L. Zhou, M. Zhang, Q. M. Luo, J. D. Glickson, B. Chance, and G. Zheng, "Two and three dimensional metabolic imaging of murine tumors using a fluorescent 2-deoxyglucose" (in preparation).
 13. B. Quistorff, J. C. Haselgrove, and B. Chance, "High spatial resolution readout of 3-D metabolic organ structure: an automated, low-temperature redox ratio-scanning instrument," *Anal. Biochem.* **148**(2), 389–400 (1985).
 14. Y. Q. Gu, Z. Y. Qian, J. X. Chen, D. Blessington, N. Ramanujam, and B. Chance, "High-resolution three-dimensional scanning optical image system for intrinsic and extrinsic contrast agents in tissue," *Rev. Sci. Instrum.* **73**(1), 172–178 (2002).
 15. B. Chance, B. Schoener, R. Oshino, F. Itshak, and Y. Nakase, "Oxidation-reduction ratio studies of mitochondria in freeze-trapped samples—nadh and flavoprotein fluorescence signals," *J. Biol. Chem.* **254**(11), 4764–4771 (1979).
 16. J. Moan and K. Berg, "The photodegradation of porphyrins in cells can be used to estimate the lifetime of singlet oxygen," *Photochem. Photobiol.* **53**(4), 549–553 (1991).
 17. Q. Peng, J. Moan, and J. M. Nesland, "Correlation of subcellular and intratumoral photosensitizer localization with ultrastructural features after photodynamic therapy," *Ultrastruct. Pathol.* **20**(2), 109–129 (1996).
 18. I. J. MacDonald, J. Morgan, D. A. Bellnier, G. M. Paszkiewicz, J. E. Whitaker, D. J. Litchfield, and T. J. Dougherty, "Subcellular localization patterns and their relationship to photodynamic activity of pyropheophorbide-a derivatives," *Photochem. Photobiol.* **70**(5), 789–797 (1999).
 19. N. L. Oleinick and H. H. Evans, "The photobiology of photodynamic therapy: cellular targets and mechanisms," *Radiat. Res.* **150**, S146–S156 (1998).
 20. B. Chance, P. Cohen, F. Jobsis, and B. Schoener, "Intracellular oxidation–reduction states in vivo," *Science* **137**, 499–508 (1962).
 21. B. B. Noodt, G. H. Rodal, M. Wainwright, Q. Peng, R. Horobin, J. M. Nesland, and K. Berg, "Apoptosis induction by different pathways with methylene blue derivative and light from mitochondrial sites in V79 cells," *Int. J. Cancer* **75**(6), 941–948 (1998).
 22. M. E. Varnes, S. M. Chiu, L. Y. Xue, and N. L. Oleinick, "Photodynamic therapy-induced apoptosis in lymphoma cells: translocation of cytochrome c causes inhibition of respiration as well as caspase activation," *Biochem. Biophys. Res. Commun.* **255**(3), 673–679 (1999).
 23. S. L. Gibson and R. Hilf, "Interdependence of fluence, drug dose and oxygen on hematoporphyrin derivative induced photosensitization of tumor mitochondria," *Photochem. Photobiol.* **42**(4), 367–373 (1985).
 24. G. Singh, W. P. Jeeves, B. C. Wilson, and D. Jang, "Mitochondrial photosensitization by photofrin II," *Photochem. Photobiol.* **46**(5), 645–649 (1987).
 25. I. Shevchuk, V. Chekulayev, J. Moan, and K. Berg, "Effects of the inhibitors of energy metabolism, lonidamine and levamisole, on 5-aminolevulinic-acid-induced photochemotherapy," *Int. J. Cancer* **67**(6), 791–799 (1996).
 26. B. W. Pogue, J. D. Pitts, M. A. Mycek, R. D. Sloboda, C. M. Wilmot, J. F. Brandsema, and J. A. O'Hara, "In vivo NADH fluorescence monitoring as an assay for cellular damage in photodynamic therapy," *Photochem. Photobiol.* **74**(6), 817–824 (2001).
 27. B. Chance and B. Thorell, "Localization and kinetics of reduced pyridine nucleotide in living cells by microfluorometry," *J. Biol. Chem.* **234**(11), 3044–3050 (1959).